Received: 21 December 2017 | Accepted: 30 April 2018

DOI: 10.1111/2041-210X.13030

RESEARCH ARTICLE

Methods in Ecology and Evolution BRITISH ECOLOGICAL SOCIETY

Using partial aggregation in spatial capture recapture

Cyril Milleret[1] | Pierre Dupont[1] | Henrik Brøseth[2] | Jonas Kindberg[2,3] | J. Andrew Royle[4] | Richard Bischof[1]

[1]Faculty of Environmental Sciences and Natural Resource Management, Norwegian University of Life Sciences, Ås, Norway

[2]Norwegian Institute for Nature Research, Trondheim, Norway

[3]Department of Wildlife, Fish, and Environmental Studies, Swedish University of Agricultural Sciences, Umeå, Sweden

[4]USGS Patuxent Wildlife Research Center, Laurel, Maryland

Correspondence
Cyril Milleret, Faculty of Environmental Sciences and Natural Resource Management, Norwegian University of Life Sciences, NO-1432 Ås, Norway.
Email: cyril.milleret@gmail.com

Funding information
Norwegian Environment Agency; Swedish Environmental Protection Agency

Handling Editor: Nigel Yoccoz

Abstract

1. Spatial capture–recapture (SCR) models are commonly used for analysing data collected using noninvasive genetic sampling (NGS). Opportunistic NGS often leads to detections that do not occur at discrete detector locations. Therefore, spatial aggregation of individual detections into fixed detectors (e.g., centre of grid cells) is an option to increase computing speed of SCR analyses. However, it may reduce precision and accuracy of parameter estimations.
2. Using simulations, we explored the impact that spatial aggregation of detections has on a trade-off between computing time and parameter precision and bias, under a range of biological conditions. We used three different observation models: the commonly used Poisson and Bernoulli models, as well as a novel way to partially aggregate detections (Partially Aggregated Binary model [PAB]) to reduce the loss of information after aggregating binary detections. The PAB model divides detectors into K subdetectors and models the frequency of subdetectors with more than one detection as a binomial response with a sample size of K. Finally, we demonstrate the consequences of aggregation and the use of the PAB model using NGS data from the monitoring of wolverine (*Gulo gulo*) in Norway.
3. Spatial aggregation of detections, while reducing computation time, does indeed incur costs in terms of reduced precision and accuracy, especially for the parameters of the detection function. SCR models estimated abundance with a low bias (<10%) even at high degree of aggregation, but only for the Poisson and PAB models. Overall, the cost of aggregation is mitigated when using the Poisson and PAB models. At the same level of aggregation, the PAB observation model out-performs the Bernoulli model in terms of accuracy of estimates, while offering the benefits of a binary observation model (less assumptions about the underlying ecological process) over the count-based model.
4. We recommend that detector spacing after aggregation does not exceed 1.5 times the scale-parameter of the detection function in order to limit bias. We recommend the use of the PAB observation model when performing spatial aggregation of binary data as it can mitigate the cost of aggregation, compared to the Bernoulli model.

KEYWORDS
partially aggregated binary model, spatial capture recapture, wolverines

1 | INTRODUCTION

Spatially explicit capture–recapture models (SCR; Efford, 2004; Borchers & Efford, 2008; Royle & Young, 2008; Royle, Chandler, Sollmann, & Gardner, 2014) are rapidly growing in popularity for ecological data analysis. SCR models are commonly used for estimating density (Bischof, Brøseth, & Gimenez, 2016; Kéry, Gardner, Stoeckle, Weber, & Royle, 2011; Royle, Magoun, Gardner, Valkenburg, & Lowell, 2011), but their scope of applications is expanding (Bischof, Steyaert, & Kindberg, 2017; Royle, Fuller, & Sutherland, 2018). Like nonspatial capture–recapture models (CR), SCR models estimate ecological parameters while accounting for imperfect detection of individuals. However, SCR models also utilize the information contained in the spatial configuration of detections and nondetections to yield spatially explicit estimates of abundance.

At their core, SCR models describe the distribution of latent activity centres (AC; centroid of an individual's activity during the time of sampling) of individuals in a population from the spatial configuration of individual detections and nondetections. SCR models couple a spatial point process model describing the spatial distribution of individual ACs with an observation model that describes the relationship between detection probability at detectors (see below for definition) and the distance from the AC. In SCR, spatial detections of individuals can be derived from a multitude of methods, from physical capture and marking, to genetic, acoustic or visual/photographic detections. These detections occur at so-called traps or, more generally, detectors. Depending on the data collection methods, detections may be associated with the point locations of physical detectors or detection devices, but could also refer to transects, irregular or gridded search areas (Efford, Borchers, & Byrom, 2009; Efford, Dawson, & Borchers, 2009; Royle, Kéry, & Guélat, 2011; Royle et al., 2014).

Spatial capture–recapture surveys, due to their spatial dimension, yield extensive detection histories (i.e., detections/nondetections of every individual at every detector). This, in turn, makes the analysis of SCR data computationally intensive (e.g., computation time), compared with nonspatial CR. This is especially true if surveys cover large areas and/or detections are recorded at high spatial resolution. For example, search-encounter methods (by foot, car or some sort of transects) generate detections from uniquely identified individuals (e.g., NGS; noninvasive genetic sampling) in a continuous space, which may result in large datasets when data are maintained at a high spatial resolution. Large SCR datasets might also concern users that wish to conduct SCR analysis with several thousands of detectors (e.g., camera traps network over large study areas). This study was motivated by our own challenge in an ongoing large carnivore monitoring programme in Scandinavia, where we aim to estimate density of wolves (*Canis lupus*), bears (*Ursus arctos*) and wolverines (*Gulo gulo*) across two countries (Norway and Sweden) spanning >700,000 km^2, using NGS data from several thousand individuals over >10 years of data collection.

The most straightforward way of coping with such large data quantities is to use some form of data summarization through spatial aggregation. For example, NGS data collected using search-encounter surveys result in detection locations in continuous space. As an alternative to modeling the continuous space search process, it is convenient to define pseudo-detectors to be the centres of grid cells of some prescribed size and then associate each detection to the closest grid cell centre (i.e., aggregation of detections to grid cells, Russell et al., 2012; Bischof, Brøseth, et al., 2016). While aggregation has the benefits of reducing the computation burden, it comes at a cost, as some information is lost in the process. When aggregating detections over grids, Russell et al. (2012) found that estimates of abundance seems to be relatively robust to the choice of grid cell size. This suggests that one could use a relatively coarse grid cell size, thereby reducing the number of detectors and increasing computing speed. From a design standpoint, there are general guidelines to keep detector spacing below a certain level relative to the home range size of studied species (see Royle et al., 2014; Sun, Fuller, & Royle, 2014). However, to our knowledge, there exists no guidelines to aggregate detections based on a formal quantification of the costs and benefits of aggregation in SCR analyses.

The two most common observation models used in SCR are the Poisson (i.e., count data) and the Bernoulli (i.e., binary data) (Bischof et al., 2017; Blanc, Marboutin, Gatti, & Gimenez, 2013; Muneza et al., 2017; Royle et al., 2014). The choice of model mostly depends on our understanding of the underlying observation process (Dawson & Efford, 2009; Royle et al., 2014). For example, when it is possible for the number of detections at a detector per occasion to be >1, then a Poisson model (or negative binomial) may be appropriate (Royle et al., 2014). Therefore, the type of data and the choice of observation model dictate the outcome of spatial aggregation of individual detections and the amount of original information preserved. Count models, such as Poisson models for detection frequency data, permit summing of individual detections across spatial units without discarding any detections. However, spatial aggregation for binary models is liable to result in a loss of information as all but the first detection of an individual within a given spatial unit are ignored.

This study has two objectives: (a) to provide quantitative information about the consequences of spatially aggregating individual detections over detectors, leading to practical guidelines for users, and (b) to introduce a novel approach—the partially aggregated binary (PAB) observation model—which reduces the loss of information arising from simple spatial aggregation of binary data through the use of a Binomial process. Although the possibility of spatially aggregating detector-level detections to form a Binomial response has been mentioned earlier (Efford, Borchers, & Mowat, 2013; Efford, Dawson, et al., 2009), to our knowledge it has neither been formalized, nor its costs and benefits formally quantified.

Using simulations, we systematically tested the effect of increasing spatial aggregation on parameter estimates using the Poisson (counts of detections of individuals), the Bernoulli (binary detections of individuals), and the PAB observation models. We simulated detections of individuals at a fine spatial scale (i.e., with a high number of detectors relative to home range size) and then aggregated detections over increasingly larger grid cells, thereby reducing the number

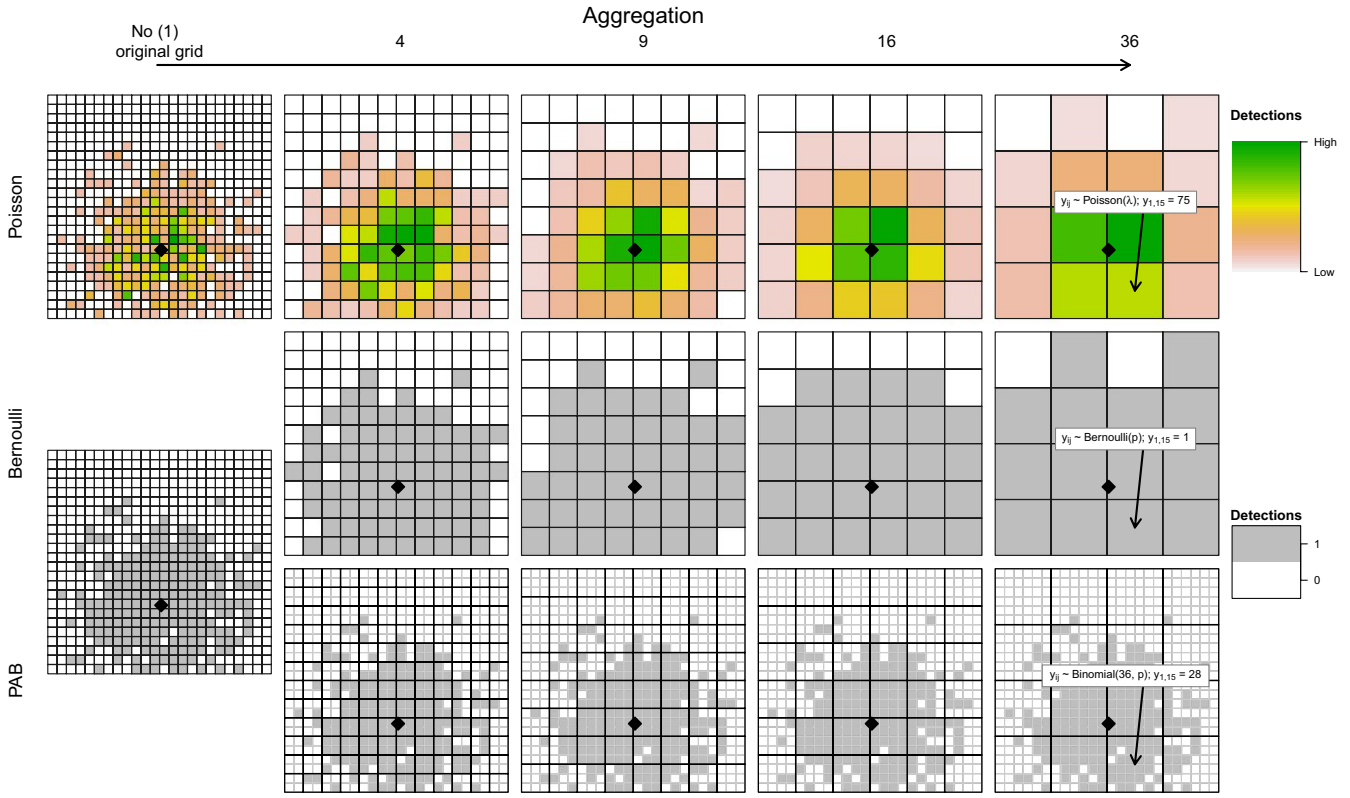

FIGURE 1 Conceptualization of spatial aggregation of detectors (represented by centroids of grid cell) with the application of a larger regular grid (*aggregated grid/primary grid*) to the original gridded detector (*original grid*). It illustrates the spatial detection of one individual (filled black diamond: activity centre) after applying Equation 7. Original detection histories before spatial aggregation are represented in the first column (No (1)), with increasing aggregation (4, 9, 16, and 36 cells) from left to right. The three different observation models considered in the analysis are shown in rows: Poisson for count (top), Bernoulli (middle) and partially aggregated binary (PAB, bottom) for binary data. The Bernoulli and PAB models are identical in the absence of aggregation. The PAB model allows for spatial aggregation of binary data without complete loss of all individual detection events at the original grid level. For illustration, the number of individual detections retained at the same detector (the 15th detector) is shown for each model type at maximum aggregation

of detectors (Figure 1). This allowed us to mimic the process that the user may follow in order to balance spatial resolution and computing speed. We then fitted SCR models to each simulated scenario and evaluated their performance (precision and bias), as well as their use of the available information and computational speed. Finally, we showcase the application of the PAB model with an empirical example: density estimation using noninvasive genetic sampling of the wolverine in Norway.

2 | MATERIALS AND METHODS

2.1 | Basic spatial capture–recapture model

The observation process describes the relationship between an individual's detection probability at a given detector and the distance $D_{i,j}$ between detector j and individual i's AC (latent variable). In our example, we considered that a detector represents any location at which an individual can be detected. We assumed that ACs were uniformly distributed within the region under study. A commonly used detection function is the half-normal, describing the probability $p_{i,j}$ of detecting individual i at detector j

$$p_{i,j} = p_0 . \exp\left(\frac{-D_{i,j}^2}{2\sigma^2}\right), \quad (1)$$

where p_0 is the expected detection probability at the AC location. The scale parameter σ can be directly linked to home range size (Royle et al., 2014) in cases where the shape of the detection function arises from the utilization distribution (home range) of the study organism. More generally, σ is related to the extent of space used over the period of study. In addition, σ could also determine the distance from which acoustic signals can be detected (Dawson & Efford, 2009). We assumed homogeneity of the parameters of the detection function across individuals and the region.

Binary detections (detection: $y = 1$; nondetection: $y = 0$) of individuals at any given detector then follow a Bernoulli distribution with probability $p_{i,j}$

$$y_{i,j} \sim Bernoulli\,(p_{i,j}) \quad (2)$$

Counts of detections can alternatively be modelled with a Poisson distribution:

$$y_{i,j} \sim Poisson\,(\lambda_{i,j}), \tag{3}$$

where $\lambda_{i,j}$, the mean number of detections of individual i at detector j, is also described using the half-normal detection function:

$$\lambda_{i,j} = \lambda_0 \cdot \exp\left(\frac{-D_{i,j}^2}{2\sigma^2}\right), \tag{4}$$

where λ_0 is the expected number of detections at the AC.

2.2 | The partially aggregated binary observation model

Spatial capture–recapture studies have used Binomial observation models as an approach to accommodate multiple temporal binary capture occasions (Efford, 2011; Royle, Karanth, Gopalaswamy, & Kumar, 2009). Using PAB, we adapted this approach to space by converting original detectors into multiple spatial binary detectors (K) associated with a new aggregated detector grid. Spatial aggregation of binary detection data leads to omission of detections, if the outcome again is to follow a Bernoulli distribution. This is because any pattern of detections and nondetections at original detectors is reduced to a single binary response during aggregation. In our example, detectors are represented in the form of grid cells but they could be defined as any other types of detectors. With the PAB observation model, each primary grid cell (aggregated detector) is subdivided into K subgrid cells (Figure 1). Then the response, the frequency of subgrid cells with at least 1 detection, is modelled as a binomial response based on a sample size of K (Figure 1, Equation 5), where K represents the number of subgrid cells within the primary grid cell.

$$y_{i,j} \sim Binomial\,(p_{i,j}, K) \tag{5}$$

This partial aggregation may be an efficient alternative to an aggregation following a Bernoulli model because it reduces the number of detectors while retaining more information about individual detections at each aggregated detector.

2.3 | Simulations

2.3.1 | SCR simulations

We simulated SCR data on a region S represented by a square polygon divided into 24 × 24 equal sized grid cells (Figure 2). For the purposes of the simulations, the centre of each of the resulting 576 cells represented a detector, with a detector spacing of 1 distance unit. We also considered a buffer around the polygon equivalent to two times σ to yield unbiased density estimates (Figure 2, Royle et al., 2014). The simulated population was demographically and geographically closed (i.e., no birth, death, immigration, or emigration during the sampling period).

We simulated a fixed number N of individuals. The location of their activity centres (ACs), s_i with geographic coordinates $s_i = (s_{xi}, s_{yi})$ for each individual i (i = 1, …, N) of the population, were uniformly and randomly distributed over the region S.

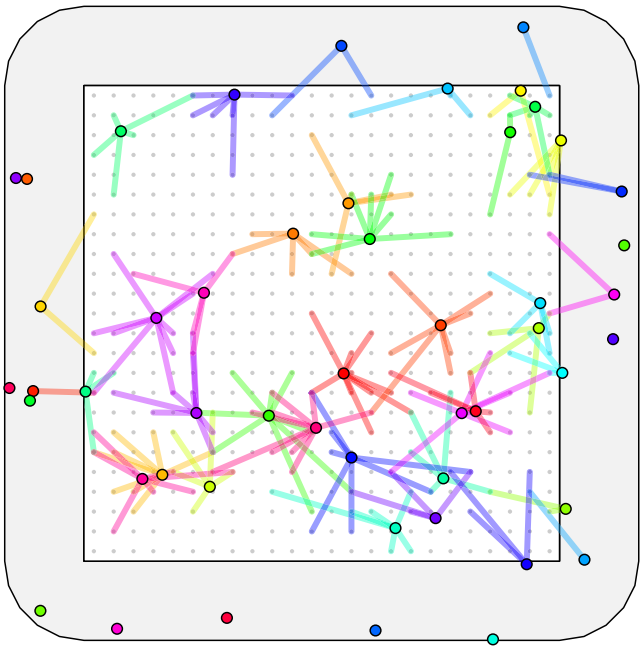

FIGURE 2 Location of individual activity centres (AC; coloured points) placed randomly within the habitat. The white polygon represents the area covered by detector grid (grey points) and the grey polygon the buffer. The Poisson observation model leads to realized counts of individual detection throughout the detector grid following the half-normal detection function (Equation 7). Detections are connected with the respective individual AC with colour-coded lines; ACs not linked to segments represent undetected individuals

$$s_i \sim Uniform\,(S) \tag{6}$$

To simulate spatially explicit detections of individuals, we set the capture probability of each individual and each detector as a function of the distance between its activity centre and the detectors using a half-normal detection function (Equation 1). We then created detection histories y for individual i at detector j by sampling from a Poisson distribution for a single temporal occasion.

$$y_{i,j} \sim Poisson\left(\lambda_0 \cdot \exp\left(\frac{-D_{i,j}^2}{2\sigma^2}\right)\right) \tag{7}$$

2.3.2 | Spatial aggregation

Once individual detections were obtained at the original high-resolution detector grid (*original grid*, Figure 1 top-left panel), we aggregated individual detections over a larger spatial unit by aggregating detectors (i.e., cells) over 4, 9, 16, and 36 cells of the original grid. This resulted in new grids (*aggregated grids*) with a corresponding detector spacing of 2, 3, 4, and 6 distance units which

exponentially decreased the number of detectors from 576 at the original grid level to 144, 64, 36, and 16 detectors (Figure 1).

We then aggregated detections consistently with the observation process represented in Figure 1: (a) for each individual, we summed all detections that occurred within aggregated grid cells for the Poisson model (Figure 1, top row); (b) we recorded whether an individual was detected at least once within an aggregated grid cell for the application of the Bernoulli observation model (also called "proximity detector" model (Efford, 2017), Figure 1, middle row); and (c) we introduced a novel way of aggregating detections for the application the PAB observation model (Figure 1, bottom row). The binary detections data at each of the original grid cells were treated as the outcomes of different Bernoulli trials, yielding a binomially distributed response at the aggregated grid level. The number of subgrids (*K*) was set as the total number of original grid cells contained in each aggregated grid cell (Figure 1).

We summed the number of detections over aggregated grid cells (*n.cells*) when aggregating the capture history for the Poisson model. Therefore, the mean of the Poisson distribution of λ_0 becomes a function of the number of aggregated cells after aggregation. We estimated the "effective" λ_0 as *n.cells** λ_0, so λ_0 can be compared among aggregation level. For the simulation sets without spatial aggregation, *n.cells* was set to 1. Additionally, because our "raw" data were simulated using a Poisson distribution (counts of detections), we used a link from the Poisson model to the Bernoulli model (Royle et al., 2014) to obtain the probability of observing a count greater than 0 for the Bernoulli and PAB models:

$$p_{i,j}\left(y_{i,j}>0\right)=1-\exp\left(-\lambda_{i,j}\right) \quad (8)$$

2.3.3 | Simulation scenarios

The scale parameter σ was set to 2 spatial grid units for all individuals, twice the minimum distance between two detectors (detector spacing) in the highest detector grid resolution (original grid). To evaluate the response of SCR models to different combinations of population and survey characteristics, we simulated populations characterized by a low (density = 0.05 per cell; *N* = 50) and high density of individuals per grid cell (density = 0.1 per cell, *N* = 100). We used 0.1 and 0.25 as baseline expected number of detections λ_0 for all detectors to yield a lower (~60%) and higher (~80%) proportion of N being detected at least once. At the original scale, aggregation was set to 4, 9, 16, and 36 cells which corresponded to 1, 1.5, 2, and 3 times σ (Figure 1).

2.4 | Data augmentation

We used data augmentation (Royle, Dorazio, & Link, 2007) to obtain an estimate of abundance (Kéry & Schaub, 2011). We augmented the dataset, so that the sum of the number of detected and augmented individuals was always equal to five times the number of simulated individuals. We associated a latent indicator z_i to every individual that reflected the probability ψ of an individual to be a member of the population. We defined z_i as a binary variable equal to 1 when an individual was a member of the population and 0 otherwise. We then obtained abundance (*N*) by summing up vector *z*.

2.5 | Model fitting

We fitted SCR models in a Bayesian framework using Markov chain Monte Carlo (MCMC) to 100 simulations for each combination of parameters. We implemented all analyses using JAGS (Plummer, 2003) with the package RJAGS (Plummer, 2016) in R version 3.3.3 (R Core Team, 2017). We ran 3,000 iterations in three chains after an adaptive phase of 1,000 iterations and thinned, so that every third iteration was retained. Models were considered to have reached convergence when the Gelman–Rubin diagnostic value *gelman.diag* function in CODA package (Brooks & Gelman, 1998; Gelman & Rubin, 1992; Plummer, Best, Cowles, & Vines, 2006) for all parameters fell below 1.1 for ≥1,000 consecutive iterations. JAGS codes for the different SCR models and simulations used are provided in Supporting Information S1 and S2. Priors and initial values are listed in Supporting Information S3, Table S3.1.

2.6 | Evaluating the performance of the models

We evaluated the performance of each SCR model in estimating abundance (*N*) and the parameters of the detection function (σ and λ_0). We quantified the relative bias ($\mathrm{RB}=\frac{1}{\theta n}\sum_{i=1}^{n}(\hat{\theta}_i-\theta)$) and the precision using the coefficient of variation ($\mathrm{CV}=\frac{SD(\hat{\theta})}{\hat{\theta}}\times 100$) (Walther & Moore, 2005), where *n* is the number of iterations, *SD* is the standard deviation, θ is the true and $\hat{\theta}$ is the estimate of the parameter obtained from MCMC. In addition, we calculated the 95% credible interval coverage as the percentage of simulations where the credible interval contained the true value. As a measure of convergence speed, we recorded the average number of iterations following the adaptive phase after which the Gelman–Rubin diagnostic value fell below 1.1 for ≥1,000 consecutive iterations. To quantify computing time for each scenario, we ran 10 iterations for 20 different simulations of each scenario on the same computer (Intel(R) Core(TM) i7-7700K CPU 4.20GHz with 62GB of ram).

2.7 | Empirical case study: The wolverines

2.7.1 | Data

We used wolverine fecal and hair samples collected by 26 different observers from the State Nature Inspectorate in Troms County (20,300 km^2) in Northern Norway. For safety reasons, observers work in pairs when snow tracking wolverines with snowmobile or on cross-country ski in the mountains in wintertime. Observers may search the same areas multiple times per winter, but areas searched do not cover the entire county. A total trail length of approximately 16,000 km was searched between February and May 2012 as a

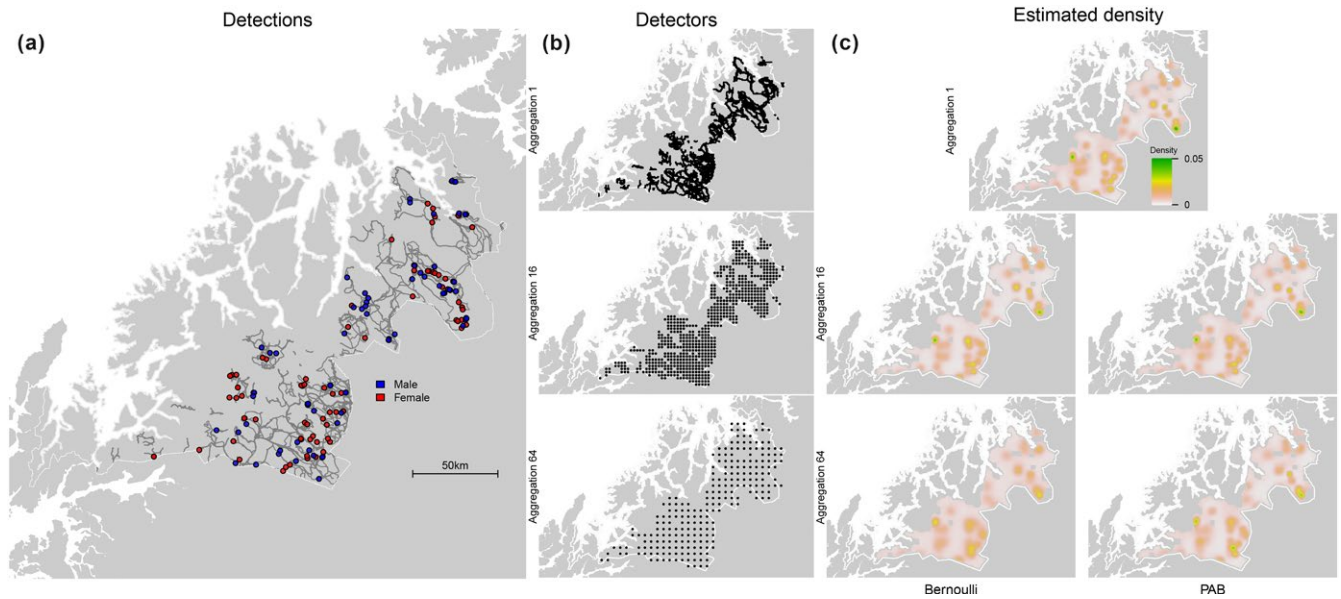

FIGURE 3 (a) Representation of the study area (within white borders; Troms, Norway) and noninvasive genetic samples from wolverines collected in 2012 (dots, red = female, blue = male) used to compute spatial capture–recapture (SCR) models. Grey lines represent search-tracks. (b) Configuration of detectors after different degrees of spatial aggregation. Aggregation 1 shows the detectors at the original grid level (detector spacing = 2 km; Number of detector = 4,551). Aggregation 16 and 64 shows detectors after aggregating grids over 16 and 64 original grid cells, and corresponds to detector spacing of 8 (658 detectors) and 16 km (233 detectors), respectively. (c) Estimated average density maps of female wolverines per 25km^2 at the original grid cell size obtained using SCR model (Aggregation1; Bernoulli) and after aggregating over 16 and 64 original grid cells using the Bernoulli and partially aggregated binary models. The density estimates presented for wolverines in Troms must be interpreted with caution, as our SCR models represent a strong simplification of the reality

part of the Norwegian Large Predator Monitoring Program. Genetic analysis was performed on all collected samples, and DNA was extracted and individuals identified using microsatellite genotyping (see Flagstad et al., 2004; Bischof, Gregersen, Brøseth, Ellegren, & Flagstad, 2016 for a complete description of the genetic analysis). As a result, the genetic ID and sex of individual wolverines, as well as spatial location of the detections were known. We used 97 (1 hair, 96 scats) and 86 (3 hair, 83 scats) detections of 44 and 27 different females and males, respectively (Figure 3a). We applied a Bernoulli and a PAB observation model while spatially aggregating the detections over grids of different coarseness (Figure 1). We started with an original grid of 4,551 detectors (i.e., searched cell centre) spaced every 2 km and then increased detector spacing to 4, 6, 8, 12, 14, and 16 km, which resulted in aggregations of detections over 4, 9, 16, 36, 49, and 64 original grid cells and led to 1,767, 994, 658, 352, 280, and 233 detectors, respectively (Figure 3b). During field collection, the coordinates of all search track logs were recorded with GPS-receivers. We considered detector grid cells that intersected a search track as detectors and as active subgrid cell (K) for the PAB models. We used a binary observation model as the basis in the empirical analysis, instead of the Poisson observation model, as the exact process by which detections accumulate may be unknown during noninvasive genetic sampling studies. In particular, scat deposition for many species is not likely to be independent and the binary observation model avoids having to specify a model for nonindependence of detection events. In such cases the binary observation model is the preferred choice of observation model (Royle et al., 2014), as all but the first detection are discarded. We therefore did not use Equation 8 and estimated p_0 instead of λ_0.

2.7.2 | Modelling

Because male wolverines tend to have larger home ranges than females (Bischof, Gregersen, et al., 2016; Persson, Wedholm, & Segerström, 2010), we fitted separate models for males and females, with a sex-specific buffer of 17 km for males and 10 km for females (i.e., approximately 2σ, as revealed by preliminary analyses). Using the PAB model, we could record the number of active original grid cells K for each aggregated grid cell. We ran 5,000 iterations of three chains after an adaptive phase of 1,000 iterations with a thinning rate of three. We considered parameter estimates from the Bernoulli model at the original grid cell size (i.e., high resolution) as the reference estimates. We then explored differences between mean parameter estimates and confidence intervals provided by the different SCR models at different level of aggregation. As during the simulations, we recorded convergence, computing speed and number of detections associated with the Bernoulli and PAB models.

3 | RESULTS

3.1 | Simulations

We ran 5,600 different models corresponding to 56 unique simulated scenarios. All models converged and 1,000 iterations were

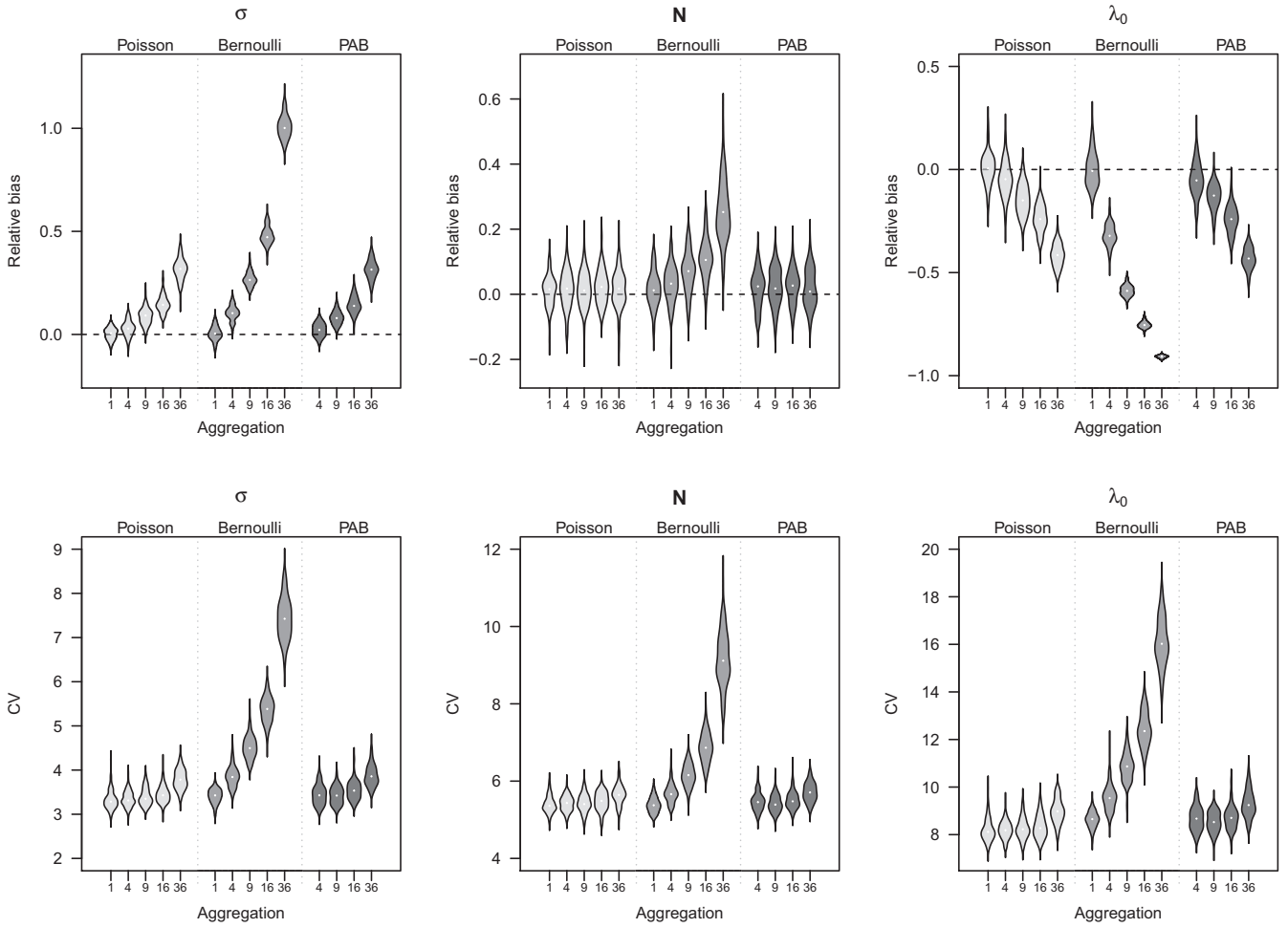

FIGURE 4 Violins plots representing the relative bias (top panels) and CV (lower panels) for σ, *N*, and λ_0 resulting from different levels of spatial aggregation of detections in spatial capture–recapture for $N = 100$ and $\lambda_0 = 0.25$. Relative width of the violins corresponds to the posterior density and white dots indicate the median of the posterior. Spatial aggregation was performed over 4, 9, 16, and 36 original grid cells and different types of data aggregation were performed to follow a Poisson, Bernoulli and partially aggregated binary (PAB) observation models. We do not show PAB violins for aggregation 1 because it is identical to the Bernoulli at aggregation 1

sufficient (Gelman–Rubin <1.1) to obtain convergence for 99.9% of the models.

3.1.1 | Parameters of the detection function (σ, λ_0)

Regardless of the type of observation model used, spatial aggregation of detections led to overestimation of σ and underestimation of λ_0. Aggregation also led to a decrease of the precision and coverage (Figure 4, Supporting Information S3, Table S3.2.A) but the magnitude and rate at which bias increased with aggregation was larger for the Bernoulli compared to the Poisson and PAB models (Figure 4, Supporting Information S3, Table S3.2.A). At large population size ($N = 100$) and high detectability ($\lambda_0 = 0.25$), the aggregation of detections over nine original cells and the use of the Bernoulli model caused a relative bias in σ that was about three times larger for the Bernoulli (0.27; *SD* = 0.03) compared to the Poisson (0.09; *SD* = 0.04) and PAB models (0.08; *SD* = 0.03; Supporting Information S3, Table S3.2.A). We observed the same pattern for the estimates of λ_0 where aggregation over nine original cells led to about four times larger (negative) relative bias. While precision of σ and λ_0 estimates (CV) was relatively constant with aggregation for the Poisson and PAB models, it increased exponentially for the Bernoulli model (Figure 4, Supporting Information S3, Table S3.2.A).

3.1.2 | Abundance (*N*)

Spatial capture–recapture models estimated *N* with no major bias and imprecision after aggregation when using the Poisson and PAB observation models (RB ≤ 0.03; CV ≤ 6; Figure 4, Supporting Information S3, Table S3.2.A). However, aggregation caused increased relative bias and decreased precision of *N* for the Bernoulli model. Relative bias in *N* was 13–26 times larger for the Bernoulli (RB = 0.26; *SD* = 0.06) compared to Poisson (RB = 0.01; *SD* = 0.06) and PAB models (*RB* = 0.02; *SD* = 0.06) when aggregating detections over 36 original cells.

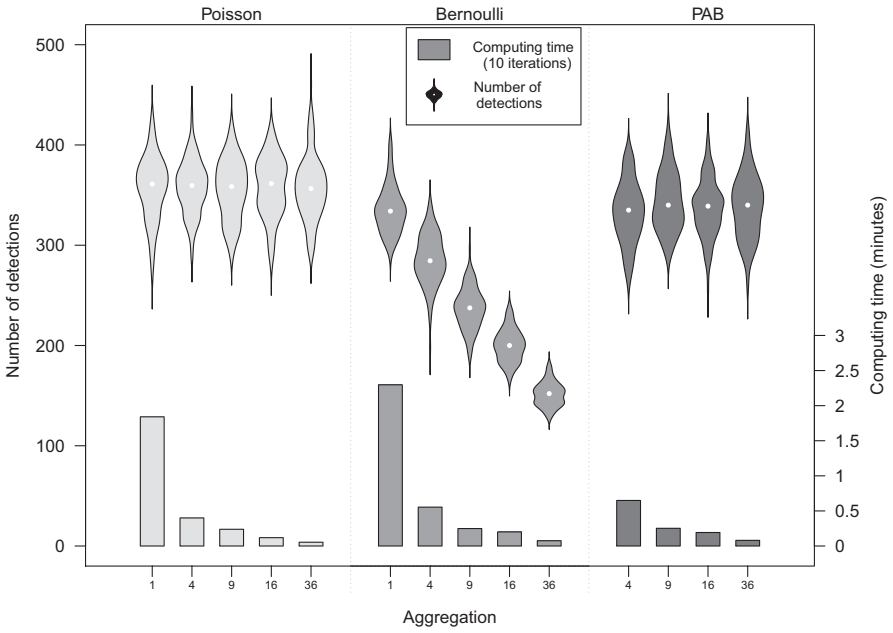

FIGURE 5 Number of detections events retained (violins) and average computing time (bars) when using the Poisson, Bernoulli and partially aggregated binary (PAB) models after different degrees of spatial aggregation of detections for the simulated data with a large population size (N = 100) and a high detectability (λ_0 = 0.25). Computing time in minutes represents average computing time (20 repetitions) necessary to run 10 iterations

3.1.3 | Computation speed and number of detections used

Computing time required for 10 iterations differed slightly between different types of models (Figure 5). However, regardless of the observation model, the time needed decreased exponentially when aggregating detectors (Figure 5). For example, on our computer, it took on average 2.15 min to run 10 iterations for the Poisson model (N = 100, λ_0 = 0.25) at the original grid level (576 detectors), while it was about five times faster (0.47 min) when aggregating detections over four grid cells (144 detectors). The Poisson and PAB observation models retained more detection events after aggregation (Figure 5).

3.1.4 | Scenarios

We observed similar patterns among all simulation scenarios. However, bias was higher at lower detection rates, and this pattern was especially pronounced for estimates of N. Precision decreased with lower detectability and when population size was low (Figure 4, Supporting Information S3, Tables S3.2.A–D and S4, Figures S4.1.A-C and S4.2).

3.2 | The wolverine

A maximum of 1,024 iterations were sufficient to obtain convergence for all models. Akin to the simulation results and despite large confidence intervals, aggregation increased the σ estimates for wolverines (Figure 6, Supporting Information S3, Table S3.3). The increase in estimated σ with aggregation was less pronounced for the PAB compared to the Bernoulli model and stronger for females compared to males (Figure 6, Supporting Information S3, Table S3.3). At the original grid cell size, σ for females was estimated to be 3.73 km with a 95% CI (3.17–4.44) that overlapped with the mean estimates obtained after aggregating detections over 64 cells for the PAB (4.38; 95% CI = 3.71–5.24) but not for the Bernoulli model (5.18; 95% CI = 4.05–6.66). N estimates had large uncertainty but were more stable with aggregation for males than for females (Figure 6, Supporting Information S3, Table S3.3).

4 | DISCUSSION

Data aggregation can significantly reduce computation time of SCR models but, as our study demonstrates, this comes at a cost. Decreasing spatial resolution of input data leads SCR models to estimate parameters with reduced precision and increased bias in cases where the detections are modelled as the result of a Poisson process and models that use a Bernoulli observation process. The increase in bias with coarser input detector grids is particularly conspicuous for the latter type of model, presumably because spatial aggregation of detectors can lead to a serious loss of information (i.e., individual detections).

Although SCR studies have used Binomial observation models as an approach to accommodate for multiple temporal binary capture occasions (Efford, 2011; Royle et al., 2009), the PAB model is, to our knowledge, the first application of the binomial model to space as it converts original detectors into multiple spatial binary detectors (K) associated with a new aggregated detector grid. Spatial aggregation of detections to fit a PAB observation model offers a practical solution to make greater use of the available data. It allows aggregation of the spatial process across a coarser grid (i.e., detectors), yet utilizing individual detections at the original detector level. We have also shown a real-life application of aggregation of detections, and the benefits of using the PAB observation model, in terms of information used and computation speed, to estimate population density and home range size of a rare and elusive species, the wolverine.

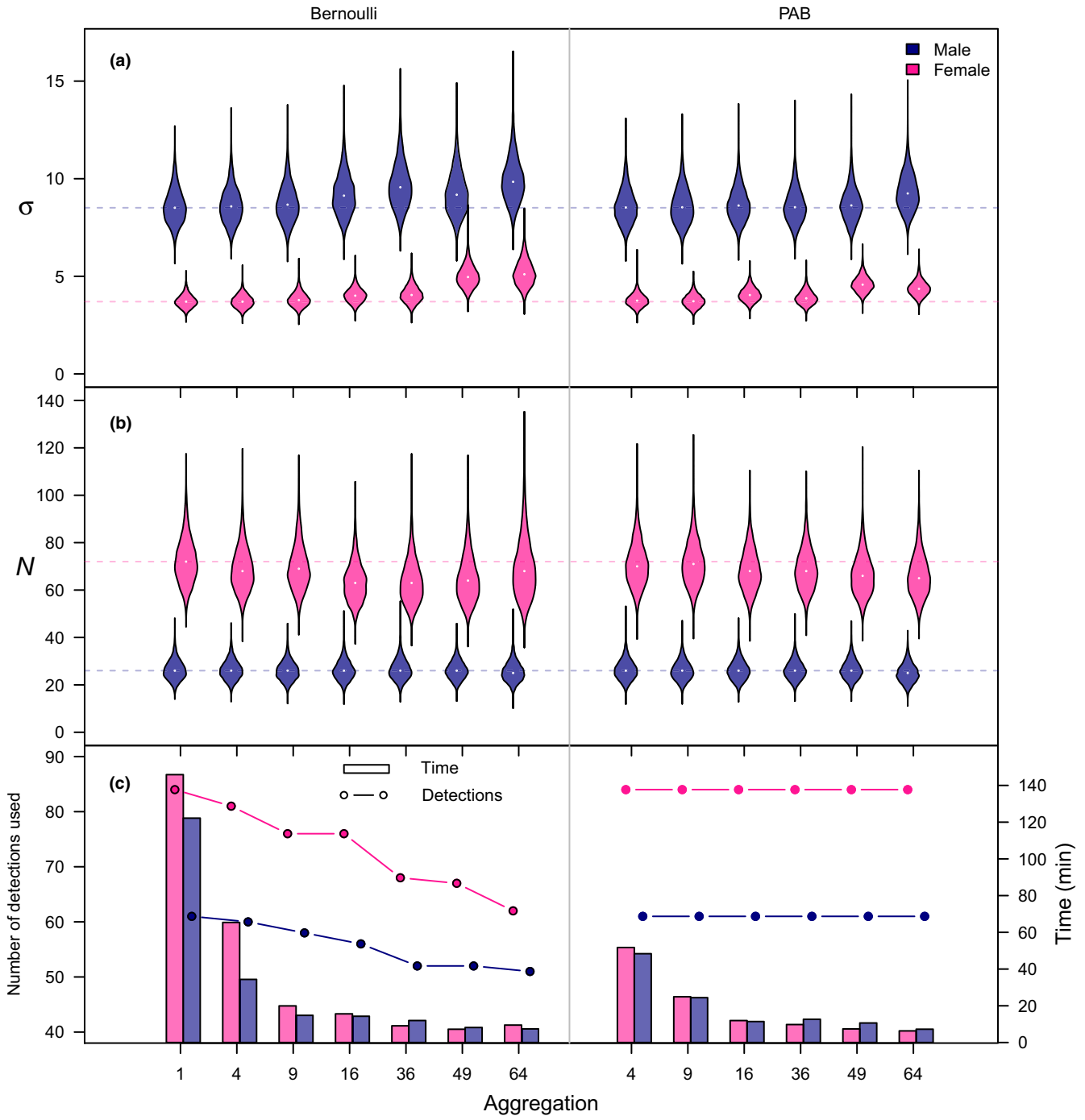

FIGURE 6 Empirical investigation of the effects of spatial aggregation of detections for noninvasive genetic sampling data from wolverines in Troms County, Norway 2012. Outcomes of spatial capture–recapture (SCR) analysis of spatially aggregating wolverine detections data over 4, 9, 16, 36, 49 and 64 cells of the original detector grid (aggregation = 1 corresponds to original grid resolution of 2×2 km^2 cell size). SCR models were fitted for Bernoulli and partially aggregated binary observation models (PAB). (a) Violin plots with posterior distributions of the scale parameter of the detection function (σ) for males (blue) and females (pink). (b) Violin plots of posterior estimates of abundance within the Troms study area and excluding the buffer area (Figure 3). Relative widths of the violins correspond to the posterior density and white dots indicate the median of the posterior. Horizontal lines represent model estimates obtained for the model without aggregation used as a reference. We do not show PAB violins for aggregation 1 because it is identical to the Bernoulli at aggregation 1. (c) The vertical bars shows the average time in minutes necessary to compute 10 iterations. The dotted line shows the number of detections utilized by each model and at a given level of aggregation. The abundance estimates presented for wolverines in Troms must be interpreted with caution, as our spatial capture–recapture models represent a strong simplification of reality

4.1 | Aggregation

Ideally, spatial aggregation of detections would not be necessary because SCR analysis could use information at its original scale and contents. However, sampling methods such as NGS, can produce data in such quantities and recorded at such a fine spatial scale that some kind of data aggregation of detections within grids might be necessary (Russell et al., 2012 but see Royle, Kéry, et al., 2011). Datasets intended for SCR analysis may have large spatial and temporal extent, therefore reducing the number of detectors through aggregation is an option to cut down on computing times. The need for computationally efficient alternatives may be particularly important as the complexity of SCR models increases, such as open population SCR models (Bischof, Brøseth, et al., 2016; Chandler & Clark, 2014).

Spatial aggregation of detections leads to projection of the true location of a detection to the nearest aggregated detector. This can result in a loss of spatial information (coarser resolution of detections) and potentially a loss of information about detections themselves, especially if a binary observation model is used. Regardless of the type of observation model used, aggregating detections over larger spatial units leads to overestimation of the observed area used by animals (Marboutin, Pruszek, Calenge, & Duchamp, 2011) and results in an overestimation of the scale parameter (σ) of SCR models. It also leads to underestimation of the baseline detection probability (λ_0).

After aggregation, SCR models estimated parameters with most severe bias for the Bernoulli observation model. Here, aggregation led to both loss of spatial resolution and detections (Figure 1). This loss of information translates into pronounced overestimation and imprecision of home range size (σ) and population size (*N*) estimated by the model. Although still conspicuous, the consequences of detector aggregation on the parameters of the detection function was less pronounced for the Poisson and PAB observation models. The choice of observation model was particularly critical for modulating the effect of aggregation on estimates of abundance. Relative bias remained low (<5%) for both the Poisson and PAB observation models, even at moderate and severe levels of aggregation.

The cost of spatial aggregation of detection can be mitigated by the choice of observation model. As demonstrated here, both the Poisson and PAB observation models outperformed the Bernoulli model with aggregation. The binary observation model has been highlighted as the model generally favoured by Royle et al. (2014), even when the sampling scheme produces detection frequencies (e.g., number of scats from an individual found at a location). One of the main reason for this choice is that repeated detections over short time intervals might not always be the result of independent detection events. Similarly, the process of local scat deposition might not always be the outcome of space usage but likely the outcome of more complex behaviors (Royle et al., 2014). Because the PAB model also uses binary detection data, we could demonstrate its use to analyse our noninvasive genetic samples from wolverines. Indeed, the PAB model is a natural extension of the Bernoulli model since it makes use of more of the raw data and use binary detections.

One of the strengths of SCR models over nonspatial CR models is the ability to yield spatially explicit predictions of abundance—density surfaces—for a study region. Although, estimates of overall abundance remained relatively unaffected by aggregation, at least for the Poisson and PAB observation models, the bias in the parameters of the detection function (σ, λ_0) suggests that high spatial aggregation of detectors may noticeably impact the degree of correspondence between predicted density surfaces and the true distribution of activity centres (Figure 3c and Supporting Information S5, Table S5.1).

4.2 | Recommendations

Our results suggest that when possible, the Poisson and PAB models should be favoured over the Bernoulli model when performing spatial aggregation. Using the PAB and Poisson models, positive bias in σ remains below an acceptable level (<10%) when spatial aggregation does not exceed areas larger than 1.5 times the σ of the studied species. However, positive bias in abundance (*N*) remains below an acceptable rate (<10%) even at high level of aggregation (up to three times σ). Our results also suggest that an overestimation and higher uncertainty in *N* are expected in study systems where individual detection probability is low (i.e., <60% of *N* detected), as it is often the case for elusive and/or rare species.

During field sampling, we recommend recording detections and search effort at the finest possible spatial resolution. While a large part of this fine scale information is lost after aggregation using the Poisson and the Bernoulli models, we can still make use of it with the PAB model. In our empirical example, we could account for the search effort in each grid, by using the number of original grid cells searched for each aggregated grid cell as a sample of size *K* in the binomial model (Equation 5). This can help account for heterogeneity in search effort that would otherwise be lost when aggregating over larger grid cells. We suggest that original grid resolution of the PAB model can be as high as desired, because a high resolution will mitigate the loss of detection with aggregation. However, according to the characteristics of the study-system the user should make sure that the resolution of the original grid cells is large enough to account for independence in the detection events, as explained above.

Determining the appropriate detector configuration before field sampling is essential in order to obtain reliable estimates of density using SCR models (Sollmann, Gardner, & Belant, 2012; Sun et al., 2014). However, due to constraints in field data collection or the type of sampling used (e.g., opportunistic sampling), detector arrays might not always be regularly spaced such as in our simulations. For our empirical study on wolverines, we tested the effect of spatially aggregating detections from irregularly located detectors (i.e., based on search tracks). Using this particular example, we demonstrated the cost of spatial aggregation on parameter estimation for individuals having small (female) and large (male) home range size. The effect of aggregation on σ was stronger for individuals having a smaller home range size. Accordingly, abundance estimates for males were more stable with aggregation than estimates obtained for females.

However, it is important to note that comparing abundance estimates when aggregating irregularly searched grids is challenging because aggregation tends to artificially increase the area covered by detectors (Figure 3b). We therefore recommend additional simulation studies to explore the effect of aggregation under different detector configuration scenarios or increased realism on the ecological and observation models (e.g., individual heterogeneity detection parameters).

5 | CONCLUSIONS

Although the computational burden of SCR is still substantial, our results show that spatially aggregating detections can be a relatively easy way to significantly reduce computational burden. At the same time, aggregating too coarsely, relative to the focal species' home range size, could lead to unacceptable compromises in terms of parameter precision and accuracy. We advise against performing large spatial aggregation using the Bernoulli model, as it can lead to highly biased parameter estimates, especially when detectability is low and few individual detections are available. On the other hand, the PAB model introduced here, can help investigators achieve the benefits of spatial aggregation in terms of computation speed, while mitigating the loss in parameter precision and accuracy associated with aggregation of binary data. Spatial aggregation could be especially helpful for studies with a large spatial extent and for complex models.

ACKNOWLEDGEMENT

This work was funded by the Norwegian Environment Agency (Miljødirektoratet) and the Swedish Environmental Protection Agency (Naturvårdsverket). We thank the field staff and members of the public that contributed to collect data for the Scandinavian large carnivore database Rovbase3.0 (rovbase.no). We thanks C. Bonenfant for help with running the models. Any use of trade, product, or firm names is for descriptive purposes only and does not imply endorsement by the U.S. Government.

AUTHORS' CONTRIBUTIONS

C.M., P.D. and R.B. conceived and designed the study, with input from H.B., J.K., J.A.R. R.B. conceived the idea of the PAB model. C.M. implemented the analysis with contributions of P.D. and R.B. H.B. and J.K. coordinated data wolverine extraction and preparation. C.M. wrote the first draft of the manuscript with help from P.D. and R.B. All authors contributed to subsequent drafts and gave final approval for publication.

DATA ACCESSIBILITY

NGS wolverine data and associated R script are available on Dryad Digital Repository https://doi.org/10.5061/dryad.pd612qp (Milleret et al., 2018).

ORCID

Cyril Milleret http://orcid.org/0000-0002-8563-981X
Pierre Dupont http://orcid.org/0000-0002-7438-7995
Henrik Brøseth http://orcid.org/0000-0003-3795-891X
Jonas Kindberg http://orcid.org/0000-0003-1445-4524
J. Andrew Royle http://orcid.org/0000-0003-3135-2167
Richard Bischof http://orcid.org/0000-0002-1267-9183

REFERENCES

Bischof, R., Brøseth, H., & Gimenez, O. (2016). Wildlife in a politically divided world: Insularism inflates estimates of brown bear abundance. *Conservation Letters*, *9*, 122–130. https://doi.org/10.1111/conl.12183.

Bischof, R., Gregersen, E. R., Brøseth, H., Ellegren, H., & Flagstad, Ø. (2016). Noninvasive genetic sampling reveals intrasex territoriality in wolverines. *Ecology and Evolution*, *6*, 1527–1536. https://doi.org/10.1002/ece3.1983

Bischof, R., Steyaert, S. M. J. G., & Kindberg, J. (2017). Caught in the mesh: Roads and their network-scale impediment to animal movement. *Ecography*, *40*, 1369–1380. https://doi.org/10.1111/ecog.02801

Blanc, L., Marboutin, E., Gatti, S., & Gimenez, O. (2013). Abundance of rare and elusive species: Empirical investigation of closed versus spatially explicit capture–recapture models with lynx as a case study. *The Journal of Wildlife Management*, *77*, 372–378. https://doi.org/10.1002/jwmg.453

Borchers, D. L., & Efford, M. G. (2008). Spatially explicit maximum likelihood methods for capture–recapture studies. *Biometrics*, *64*, 377–385. https://doi.org/10.1111/j.1541-0420.2007.00927.x

Brooks, S. P., & Gelman, A. (1998). General methods for monitoring convergence of iterative simulations. *Journal of Computational and Graphical Statistics*, *7*, 434–455.

Chandler, R. B., & Clark, J. D. (2014). Spatially explicit integrated population models. *Methods in Ecology and Evolution*, *5*, 1351–1360. https://doi.org/10.1111/2041-210X.12153

Dawson, D. K., & Efford, M. G. (2009). Bird population density estimated from acoustic signals. *Journal of Applied Ecology*, *46*, 1201–1209. https://doi.org/10.1111/j.1365-2664.2009.01731.x

Efford, M. G. (2004). Density estimation in live-trapping studies. *Oikos*, *106*, 598–610. https://doi.org/10.1111/j.0030-1299.2004.13043.x

Efford, M. G. (2011). Estimation of population density by spatially explicit capture–recapture analysis of data from area searches. *Ecology*, *92*, 2202–2207. https://doi.org/10.1890/11-0332.1

Efford, M. G. (2017). secr: Spatially explicit capture–recapture models.

Efford, M. G., Borchers, D. L., & Byrom, A. E. (2009). Density estimation by spatially explicit capture–recapture: Likelihood-based methods. In D. L. Thomson, E. G. Cooch, & M. J. Conroy (Eds.), *Modeling demographic processes in marked populations* (pp. 255–269). Boston, MA: Springer US. https://doi.org/10.1007/978-0-387-78151-8

Efford, M. G., Borchers, D. L., & Mowat, G. (2013). Varying effort in capture–recapture studies. *Methods in Ecology and Evolution*, *4*, 629–636. https://doi.org/10.1111/2041-210X.12049

Efford, M. G., Dawson, D. K., & Borchers, D. L. (2009). Population density estimated from locations of individuals on a passive detector array. *Ecology*, *90*, 2676–2682. https://doi.org/10.1890/08-1735.1

Flagstad, Ø., Hedmark, E., Landa, A., Brøseth, H., Persson, J., Andersen, R., … Ellegren, H. (2004). Colonization history and noninvasive monitoring of a reestablished wolverine population. *Conservation Biology*, *18*, 676–688. https://doi.org/10.1111/j.1523-1739.2004.00328.x-i1

Gelman, A., & Rubin, D. B. (1992). Inference from iterative simulation using multiple sequences. *Statistical Science*, *7*, 457–511. https://doi.org/10.1214/ss/1177011136

Kéry, M., Gardner, B., Stoeckle, T., Weber, D., & Royle, J. A. (2011). Use of spatial capture–recapture modeling and DNA data to estimate densities of elusive animals. *Conservation Biology*, *25*, 356–364.

Kéry, M., & Schaub, M. (2011). *Bayesian population analysis using WinBUGS: A hierarchical perspective*. Waltham, MA: Academic Press.

Marboutin, E., Pruszek, M., Calenge, C., & Duchamp, C. (2011). On the effects of grid size and shape when mapping the distribution range of a recolonising wolf (*Canis lupus*) population. *European Journal of Wildlife Research*, *57*, 457–465. https://doi.org/10.1007/s10344-010-0453-2

Milleret, C., Dupont, P., Brøseth, H., Kindberg, J., Royle, J. A., & Bischof, R. (2018). Data from: Using partial aggregation in spatial capture recapture. *Dryad Digital Repository*, https://doi.org/10.5061/dryad.pd612qp

Muneza, A. B., Linden, D. W., Montgomery, R. A., Dickman, A. J., Roloff, G. J., Macdonald, D. W., & Fennessy, J. T. (2017). Examining disease prevalence for species of conservation concern using non-invasive spatial capture–recapture techniques. *Journal of Applied Ecology*, *54*, 709–717. https://doi.org/10.1111/1365-2664.12796

Persson, J., Wedholm, P., & Segerström, P. (2010). Space use and territoriality of wolverines (*Gulo gulo*) in northern Scandinavia. *European Journal of Wildlife Research*, *56*, 49–57. https://doi.org/10.1007/s10344-009-0290-3

Plummer, M. (2003). JAGS; a program for analysis of Bayesian graphical models using Gibbs Sampling. R project for statistical computing. *Proceedings of the third international workshop on distributed statistical computing*, Vienna, Austria.

Plummer, M. (2016). RJAGS: Bayesian graphical models using MCMC.

Plummer, M., Best, N., Cowles, K., & Vines, K. (2006). CODA: Convergence diagnosis and output analysis for MCMC. *R News*, *6*, 7–11.

R Core Team. (2017). *R: A language and environment for statistical computing*. Vienna, Austria: R Foundation for Statistical Computing. URL https://www.R-project.org/.

Royle, J. A., Chandler, R. B., Sollmann, R., & Gardner, B. (2014). *Spatial capture–recapture*. Waltham, MA: Elsevier, Academic Press.

Royle, J. A., Dorazio, R. M., & Link, W. A. (2007). Analysis of multinomial models with unknown index using data augmentation. *Journal of Computational and Graphical Statistics*, *16*(1), 67–85. https://doi.org/10.1198/106186007X181425

Royle, J. A., Fuller, A. K., & Sutherland, C. (2018). Unifying population and landscape ecology with spatial capture–recapture. *Ecography*, *41*, 444–456. https://doi.org/10.1111/ecog.03170

Royle, J. A., Karanth, K. U., Gopalaswamy, A. M., & Kumar, N. S. (2009). Bayesian inference in camera trapping studies for a class of spatial capture–recapture models. *Ecology*, *90*, 3233–3244. https://doi.org/10.1890/08-1481.1

Royle, J. A., Kéry, M., & Guélat, J. (2011). Spatial capture–recapture models for search-encounter data. *Methods in Ecology and Evolution*, *2*, 602–611. https://doi.org/10.1111/j.2041-210X.2011.00116.x

Royle, J. A., Magoun, A. J., Gardner, B., Valkenburg, P., & Lowell, R. E. (2011). Density estimation in a wolverine population using spatial capture–recapture models. *The Journal of Wildlife Management*, *75*, 604–611. https://doi.org/10.1002/jwmg.79

Royle, J. A., & Young, K. V. (2008). A hierarchical model for spatial capture–recapture data. *Ecology*, *89*, 2281–2289. https://doi.org/10.1890/07-0601.1

Russell, R. E., Royle, J. A., Desimone, R., Schwartz, M. K., Edwards, V. L., Pilgrim, K. P., & Mckelvey, K. S. (2012). Estimating abundance of mountain lions from unstructured spatial sampling. *The Journal of Wildlife Management*, *76*, 1551–1561. https://doi.org/10.1002/jwmg.412

Sollmann, R., Gardner, B., & Belant, J. L. (2012). How does spatial study design influence density estimates from spatial capture–recapture models? *PLoS ONE*, *7*, 1–8.

Sun, C. C., Fuller, A. K., & Royle, J. A. (2014). Trap configuration and spacing influences parameter estimates in spatial capture–recapture models. *PLoS ONE*, *9*, 1–9 https://doi.org/10.1371/journal.pone.0088025.

Walther, B. A., & Moore, J. L. (2005). The concepts of bias, precision and accuracy, and their use in testing the performance of species richness estimators, with a literature review of estimator performance. *Ecography*, *28*, 815–829. https://doi.org/10.1111/j.2005.0906-7590.04112.x

SUPPORTING INFORMATION

Additional supporting information may be found online in the Supporting Information section at the end of the article.

How to cite this article: Milleret C, Dupont P, Brøseth H, Kindberg J, Royle JA, Bischof R. Using partial aggregation in spatial capture recapture. *Methods Ecol Evol*. 2018;00:1–12. https://doi.org/10.1111/2041-210X.13030